Effect of Photoanode Design on the Photoelectrochemical Performance of Dye-Sensitized Solar Cells Based on SnO? Nanocomposite

Authors:

I-Ming Hung, Ripon Bhattacharjee

Date Submitted: 2019-01-30

Keywords: dye-sensitized solar cells (DSSCs), nanocomposite, nanoflower, nanoparticle, photoanode

Abstract:

Li-doped ZnO (LZO) aggregated nanoparticles are used as an insulating layer in SnO? nanocomposite (SNC) photoanodes to suppress the recombination process in dye-sensitized solar cells (DSSCs). Various weight percentages of SnO? nanoparticles (SNPs) and SnO? nanoflowers (SNFs) were used to prepare SNC photoanodes. The photocurrent-voltage characteristics showed that the incorporation of an LZO insulating layer in an SNC photoanode increased the conversion efficiency of DSSCs. This was due to an increase in the surface area, charge injection, and charge collection, and the minimization of the recombination rate of photoanodes. Electrochemical impedance spectroscopy (EIS) results showed lower series resistance, charge injection resistance, and shorter lifetimes for DSSCs based on an SNC photoanode with an LZO insulating layer. The open circuit voltage and fill factor of the DSSCs based on SNC photoanodes with an LZO insulating layer significantly increased. The DSSC based on a SNC photoanode with a SNC:SNF weight ratio of 1:1 had a high current density of 4.73 mA/cm², open circuit voltage of 630 mV, fill factor of 69%, and efficiency of 2.06%.

Record Type: Published Article

Submitted To: LAPSE (Living Archive for Process Systems Engineering)

Citation (overall record, always the latest version):	LAPSE:2019.0149
Citation (this specific file, latest version):	LAPSE:2019.0149-1
Citation (this specific file, this version):	LAPSE:2019.0149-1v1

DOI of Published Version: https://doi.org/10.3390/en9080641

energies

MDPI

Article

Effect of Photoanode Design on the Photoelectrochemical Performance of Dye-Sensitized Solar Cells Based on SnO_2 Nanocomposite

I-Ming Hung * and Ripon Bhattacharjee

Department of Chemical Engineering and Materials Science, Yuan Ze University, Taoyuan 32003, Taiwan; ripon_cep@yahoo.com

* Correspondence: imhung@saturn.yzu.edu.tw; Tel.: +886-3-463-8800 (ext. 2569)

Academic Editor: Issouf Fofana

Received: 2 June 2016; Accepted: 8 August 2016; Published: 13 August 2016

Abstract: Li-doped ZnO (LZO) aggregated nanoparticles are used as an insulating layer in SnO_2 nanocomposite (SNC) photoanodes to suppress the recombination process in dye-sensitized solar cells (DSSCs). Various weight percentages of SnO_2 nanoparticles (SNPs) and SnO_2 nanoflowers (SNFs) were used to prepare SNC photoanodes. The photocurrent-voltage characteristics showed that the incorporation of an LZO insulating layer in an SNC photoanode increased the conversion efficiency of DSSCs. This was due to an increase in the surface area, charge injection, and charge collection, and the minimization of the recombination rate of photoanodes. Electrochemical impedance spectroscopy (EIS) results showed lower series resistance, charge injection resistance, and shorter lifetimes for DSSCs based on an SNC photoanode with an LZO insulating layer. The open circuit voltage and fill factor of the DSSCs based on SNC photoanodes with an LZO insulating layer significantly increased. The DSSC based on a SNC photoanode with a SNC:SNF weight ratio of 1:1 had a high current density of 4.73 mA/cm^2, open circuit voltage of 630 mV, fill factor of 69%, and efficiency of 2.06%.

Keywords: photoanode; nanoparticle; nanoflower; nanocomposite; dye-sensitized solar cells (DSSCs)

1. Introduction

Dye-sensitized solar cells (DSSCs) have been considered a cost effective, environmentally friendly alternative power source since 1991. The redox mediators based on cobalt complexes allowed DSSCs to achieve efficiencies exceeding 14% and the science community has recently proposed various approaches and materials to increase the stability of DSSCs [1]. Various morphologies of nanoparticles, nanowires, and nanoflowers in DSSC reduce the fabrication cost, stabilize the structure of materials, and provide high light absorption and electron collection [2]. The novelty and flexible portable DSSCs were prepared to compete the traditional silicon solar cell due to the low cost and easy-to-prepare materials [3]. In addition, a new photoelectrochromic device which is the combination of electrochromic device and a polymer-based DSSC was reported and shows long-term stability under real outdoor conditions [4]. Recently, many studies have focused on metal oxide photoanodes, such as TiO_2 [5], ZnO [6], SnO_2 [7], and Zn_2SnO_3 [8]. Among them, SnO_2 are the most prominent candidate, due to its optical and electrical properties, such as higher electronic mobility [9] wide band gap energy as compared to TiO_2, which also guarantees higher stability under ultraviolet-visible (UV) illumination [10].

However, DSSCs based on SnO_2 photoanode materials exhibit relatively low open circuit voltages because of their high recombination kinetics with electrolytes [11]. In addition, they reduce the conversion efficiency. SnO_2 with various morphologies of nanograin [4], nanowires [11], and nanoparticles [12] have been investigated to increase the photoconversion efficiency of SnO_2-based

DSSCs. The high recombination rate and poor electron transfer efficiency in SnO_2-based DSSCs are still major challenges for increasing the energy conversion efficiency.

Coating a high band gap material, such as Zn_2SnO_4 [13], ZnO [14], or MgO [15], on the surface of SnO_2 is a promising method to reduce the recombination rate and increase the charge collection in DSSCs. During the SnO_2 coating with different band gap semiconductor materials, the electron density in the conduction band of SnO_2 increases and the charge recombination decreases because of the core-shell barrier. Therefore, the open circuit voltage and the conversion efficiency of solar cells increase. However, the effect of the insulating layer on the conversion efficiency of DSSC requires further investigation. The satisfactory crystallization and electrical conduction of ZnO materials can be used as an insulating layer for SnO_2-based DSSCs. The different conduction band energy [16] and higher electron mobility of ZnO compared with SnO_2 could minimize the interfacial charge recombination and redox species oxidation in the electrolyte and solid-state hole transporter. However, the low specific surface area of ZnO films and the formation of an inactive Zn^{2+}/dye complex layer on the ZnO surface reduce the injection efficiency of electrons from the dye molecules to the lower semiconductor. To suppress the recombination process in DSSCs, numerous studies on modifying ZnO by doping various elements, such as Sn [17], Mg [18], and Li [19] have been conducted. In addition, ZnO with different morphologies, such as nanorods, nanoflowers, nanotubes, nanowires, and nanofibers for DSSC photoelectrodes have been prepared and shown showed a significant effect on the energy efficiency of DSSC [20]. Microspherical particles with nanocrystallites are believed to have numerous favorable properties, including high specific surface area and effective scattering properties. Therefore, the Li-ZnO microspherical structure is expected to provide a high dye adsorption amount and light scattering properties to increase the energy conversion efficiency of DSSCs. Even the nanomaterials can improve the performance of the DSSCs, however, it is well known that many nanoparticles, such as TiO_2, ZnO, SnO_2, Ag, etc., can cause significant toxic effects in animal tissues, cells or plant species [21–23]. Therefore, it is important to have a careful standard operating proceedure for the preparation and recycling of DSSCs based on nano-structure materials.

In a previous study [24], we reported the deposition of a ZnO layer onto SnO_2 material, which improved the cell conversion efficiency by more than two-fold. In this study, the SnO_2 nanocomposites (SNCs), with various weight ratios of SnO_2 nanoparticles (SNPs) and SnO_2 nanoflowers (SNFs) were prepared and coated on Li-doped ZnO (LZO) aggregated nanoparticles, which were used as insulating layers on the top of SNC (SNC_Z). The recombination process in SNC and SNC_Z photoanodes were investigated in detail by using open circuit voltage decay (OCVD) and dark current and electrochemical impedance spectroscopy (EIS) methods.

2. Results and Discussion

The scanning electron microscope (SEM) top and cross-sectional views of the SNC photoanodes with various weight percentages of SNPs and SNFs are shown in Figure 1. SEM micrographs show that the SNFs with a 1.4–1.9 μm diameter uniformly mixed with the SNPs and the average thickness of the SNC samples was approximately 3.2 μm. The cross-sectional view is shown in Figure 1f; an SNP layer with a thickness of 1.4 μm on the top of a fluorine-doped SnO_2 (FTO) substrate was an interconnector between the FTO and SNF nanostructures. Figure 1c,d shows the top and cross-sectional views; the SNFs were clearly observed as the weight ratio of SNFs was increased to exceed that of SNPs. The inset high-magnification micrographs in Figure 1c,d show that the SNPs were firmly attached to the SNFs and well interconnected to SNFs and the substrate. Figure 2 shows the SEM micrographs of the LZO nanoparticles on the top of the SNC photoanodes. The SEM micrographs revealed that the size of the uniform LZO spheres ranged from 750 nm to 1.25 μm. The high surface area of these LZO particles were due to their rough surface and were expected to improve the light scattering properties and increase the dye absorption of the photoanodes.

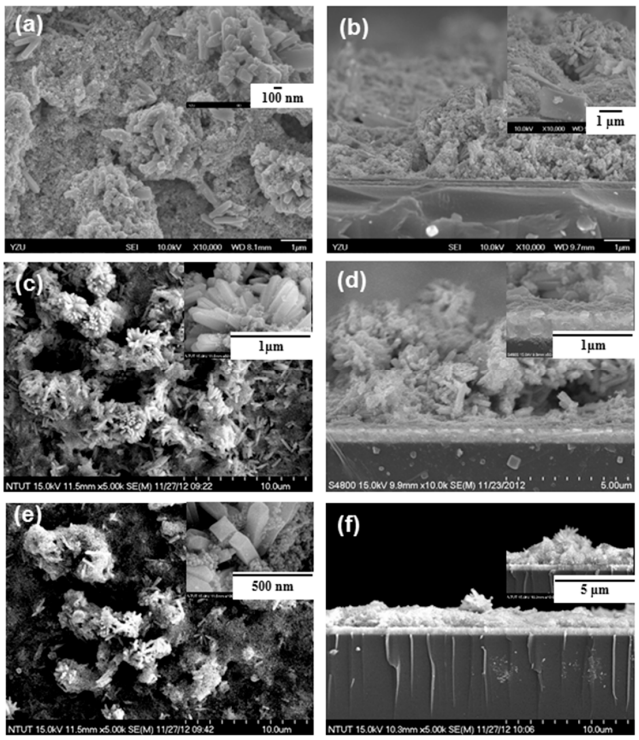

Figure 1. Scanning electron microscope (SEM) micrographs of (**a**) SnO_2 nanocomposite (SNC) (1:1); (**c**) SNC (1:0.5); and (**e**) SNC (0.5:1) top views; and (**b**), (**d**), and (**f**) cross-sectional views. The inset micrographs are corresponding high magnification views.

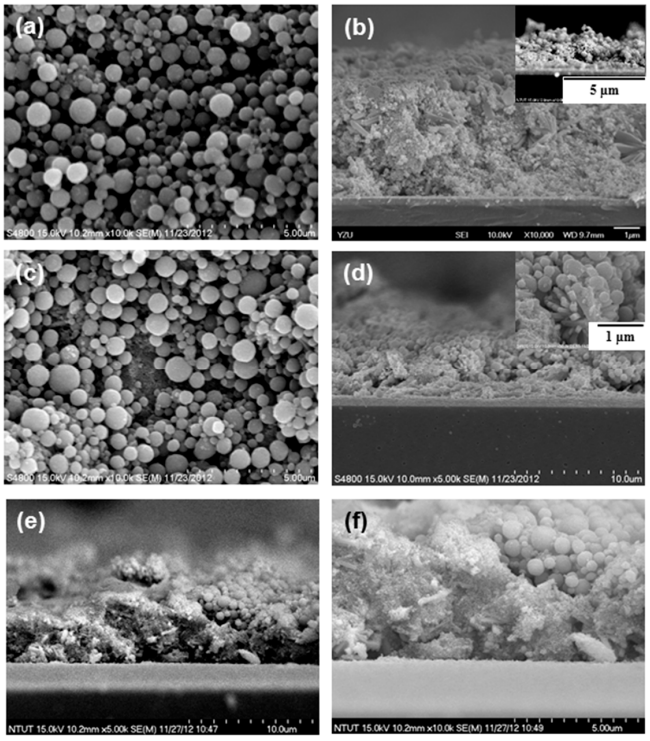

Figure 2. SEM micrographs of (**a**) SNC_Z (1:1) and (**c**) SNC_Z (1:0.5) top views; (**b**) SNC_Z (1:1) and (**d**) SNC_Z (1:0.5) cross-sectional views; (**e**) and (**f**) are the cross-sectional views of the SNC_Z (0.5:1) photoanodes.

Figure 3 shows the X-ray diffractometer (XRD) patterns of SNF, SNC (1:1), and SNC_Z (1:1) photoanodes annealed at 450 °C for 2 h. All the diffraction peaks of SNF and SNC (1:1) were perfectly indexed as the tetragonal rutile SnO_2 structure (JCPDS No. 41-1445). In the case of SNC_Z (1:1), the diffraction peaks were related to ZnO (JCPDS No. 36-1451) and SnO_2 (JCPDS No. 41-1445). No second phases were detected in the SNC_Z (1:1) sample, indicating that there was no chemical reaction between ZnO and SnO_2 at 450 °C.

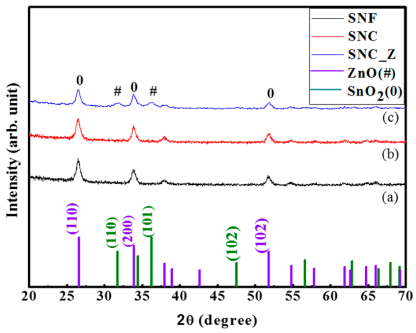

Figure 3. X-ray diffractometer (XRD) patterns of (**a**) SnO_2 nanoparticle (SNP); (**b**) SnO_2 nanoflower (SNF); and (**c**) SNC_Z (1:1) samples.

Figure 4 and Table 1 show the *J-V*, photo-to-current conversion efficiency (*IPCE*) curves, and the characteristics of the DSSCs based on SNC photoanodes with and without the LZO layer. Among SNC (1:0.5), SNC (1:1), and SNC (0.5:1) photoanodes, the SNC (1:1) photoanode showed a higher V_{oc}, fill factor (*FF*), *IPCE*, and energy conversion efficiency (η) than the SNC (1:0.5) and SNC (0.5:1) photoanodes. However, without the LZO layer (only SNC), the J_{sc}, V_{oc}, *FF*, *IPCE*, and η were lower than those of the DSSCs based on the SNC_Z photoanodes (with LZO). Comparing with the performance of the DSSCs based on the SNC (1:1) photoanode, the J_{sc} and V_{oc} of the DSSCs-based on the SNC_Z (1:1) photoanode increased from 2.21 mA/cm^2 to 4.73 mA/cm^2, and from 549 mV to 630 mV, respectively. The apparent increased V_{oc} of DSSCs based on the SNC_Z photoanodes indicated that the electron recombination rate was low because of the LZO layer coated on the top of the SNC photoanodes. The open circuit potential of DSSC is directly related to the concentration of electrons in the conduction band. This concentration is mainly limited by the recombination of conduction band electrons with I_3^- ions in the electrolyte and oxidized dye molecules. The recombination of the conduction band electrons with oxidized dye molecules was negligible; therefore, this process was significantly slower than the regeneration of the sensitizer by I_3^- [25]. Significant improvement of the *FF* and *IPCE* from 57.38% to 69.33%, and from 57.3% to 78.5%, respectively, caused the η of the SNC photoanode coated with the LZO layer DSSCs increased from 0.7% to 2.06% (approximately three times), which is higher than that of the DSSCs based on the SnO_2 photoanode [26].

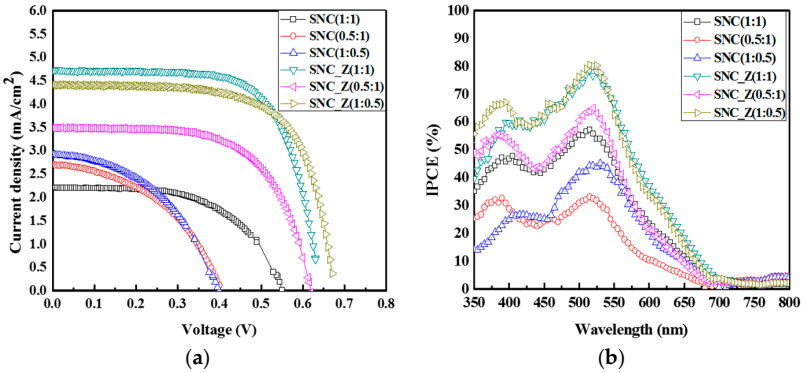

Figure 4. (**a**) *I-V* characteristic curves; and (**b**) photo-to-current conversion efficiency (*IPCE*) curves of the dye-sensitized solar cells (DSSCs) based on different photoanodes.

Table 1. Photoelectrochemical performance of the DSSCs based on different photoanodes.

Sample	J_{sc} (mA/cm^2)	V_{oc} (mV)	*FF* (%)	*IPCE* (%)	η (%)
SNC (1:1)	2.21	549.93	57.38	57.3	0.70
SNC (1:0.5)	2.91	395.13	45.92	44.4	0.65
SNC (0.5:1)	2.72	400.07	45.00	33.0	0.49
SNC_Z (1:1)	4.73	630.15	69.33	78.5	2.06
SNC_Z (1:0.5)	3.57	670.16	68.56	80.6	2.02
SNC_Z (0.5:1)	3.49	615.08	63.21	63.9	1.36

The electron leakages in DSSCs were mainly caused by a back-electron transfer process; for instance, the electrochemical reduction of I_3^- at the FTO surface [27]. The conversion efficiency of the DSSCs could be increased by restraining the back-electron transfer process. Dark current can explain this electrochemical behavior regarding the back-charge transfer process in the DSSCs. The dark current obtained by sweeping the potential bias from 0 V to 1.0 V for different DSSCs are shown in Figure 5. Under the dark condition, the current originated from the reduction of I_3^- at the surface of the FTO substrate [28]. In addition, the onset potential of the DSSCs based on the SNC_Z photoanodes is lower than that of the DSSCs based on SNC photoanodes. The onset potential of the DSSCs based on the SNC_Z (0.5:1) photoanode is 610 mV, whereas that of the DSSCs based on the SNC (0.5:1) photoanode is 380 mV. The reduction current of the DSSCs based on SNC_Z photoanodes decreased significantly compare with that of the DSSCs based on SNC photoanodes because the potential is > 500 mV. This indicated that the different band gap between ZnO and SnO_2 reduced the reaction sites for the charge recombination of the electrons originating from the FTO substrate and I_3^- ions in the electrolyte [29]. The onset potential of the DSSCs based on the SNC_Z (1:0.5) photoanode increased from 350 mV to 600 mV, compare to the DSSCs based on the SNC (1:0.5) photoanode. The increase in the onset potential indicated a lower recombination in the SNC_Z photoanode than in the SNC photoanodes. The increase in the V_{oc} of DSSCs based on the SNC_Z photoanodes caused by the LZO insulating layer sufficiently decreased the interfacial electron recombination phenomenon. The higher electron concentration in the conduction band and the reduction of the recombination rate improved the photo-electrochemical performance of the DSSCs.

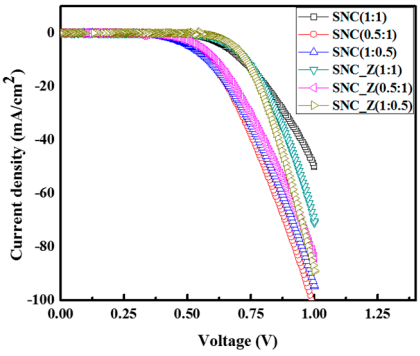

Figure 5. Dark current characteristics of the DSSCs based on different photoanodes.

The increase in V_{oc} is always related to a negative shift in the conduction band or the suppression of the charge recombination [30]. The increase in the dark current caused by the I_3^- ions generated electrons from the semiconductor and reduce to iodine. The conduction band position of SnO_2 is lower than that of ZnO [31], causing the dye molecules, which were absorbed on in ZnO, to inject the electron into the conduction band of LZO, and the electron then passed through the interlinked SnO_2 particles. The energy of the LZO-SnO_2 heterojunction is schematically shown in Figure 6. This photoanode microstructure design is useful for separating the negative and positive charges and reducing the injected electron recombination between the photoanode material with the redox I_3^-/I^- and the oxide

dye. The concept of using SnO_2 nanoflowers and nanoparticles was to improve the interconnection between each layers and implement it into a DSSC. Better interconnection can improve the device stability and faster charge transfer [22]. The recombination process in a DSSC was suppressed using this new structure and we were able to minimize that process and improve the device performance three-fold compared to a simple SnO_2 photoanode.

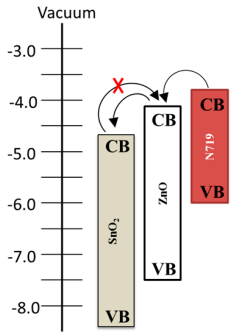

Figure 6. Schematic diagram of electron transfer mechanism for the SnO_2/ZnO nanocomposite photoanode.

OCVD measurements have been widely used to obtain the electron lifetime (τ_e) of DSSCs; these measurements contains useful information on the rate constants of the electron transfer process [32]. The OCVD technique was used to monitor the subsequent decay of photovoltage after turning off the illumination. Figure 7a shows the voltage decay curves of the DSSCs based on SNC and SNC_Z photoanodes and the calculated τ_e using Equation (1) [33,34]:

$$\tau_e = -\frac{K_B T}{e}\left(\frac{dV_{oc}}{dt}\right)^{-1} \quad (1)$$

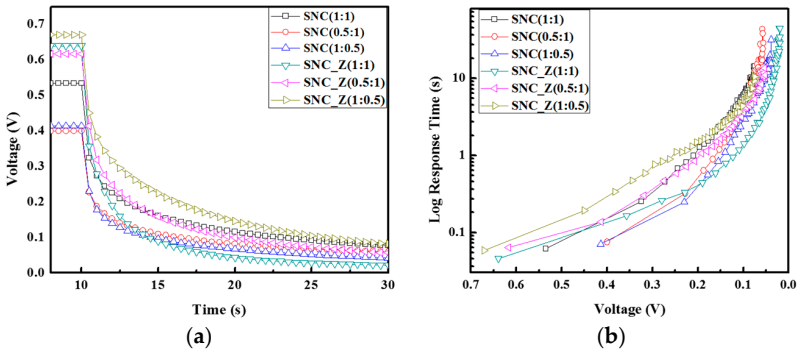

Figure 7. (**a**) Open circuit voltage decay; and (**b**) electron lifetime of the DSSCs based on different photoanodes.

The response time in the low-voltage region depends on the surface trap density in the photoanode [35]. The OCVD results show that the response time in the DSSCs based on the SNC_Z (1:0.5) photoanode is higher than that in the DSSCs based on the SNC photoanode in the low V_{oc} region, indicating that the SNC_Z (1:0.5) photoanode has a higher surface trap density than that without the LZO layer. Figure 7b shows the electron lifetimes as a function of voltage; the electron lifetime in the SNC_Z photoanode is longer than that in the SNC photoanode. The longer electron lifetime in the SNC photoanodes with the LZO layer indicated a lower charge recombination rate; therefore, the SNC_Z photoanodes were expected to have a higher energy conversion efficiency [32]. This increase in the electron transfer efficiency is clearly caused by the optimized electron transfer

pathways in the modified microstructure of the photoanodes. The expected electron transfer network was successfully constructed and is shown in Figure 2. The inter-particle connection incorporated into the LZO coating layer on the SNC surface and the FTO substrate. This photoanode microstructure caused the electrons in the conduction band to move to the external circuit through the shortest pathway. The shortest pathway for electron transfer reduced the probability of the electrons being recaptured and considerably increased the transfer velocity of the photo-generated electrons from the conduction band to the external circuit.

To further clarify the relationship between the photovoltaic performance of the SNC photoanodes with and without the LZO insulating layer, EIS was used to evaluate the charge transport and collection in the photoanode. The conversion performance of the DSSCs can be improved by increasing the dye adsorption amount and electron transport based on the optimized morphology or thickness of the photoanodes [35,36]. However, Guerin et al. [37] reported that reduction of the electron lifetime in a photoanode is a crucial factor for obtaining high efficiency in DSSCs. Therefore, we studied the charge transport and collection in detail to explain the increase in the energy conversion efficiency of DSSCs. EIS spectra and photovoltage-current transient measurements are shown in Figure 8 and summarized in Table 2.

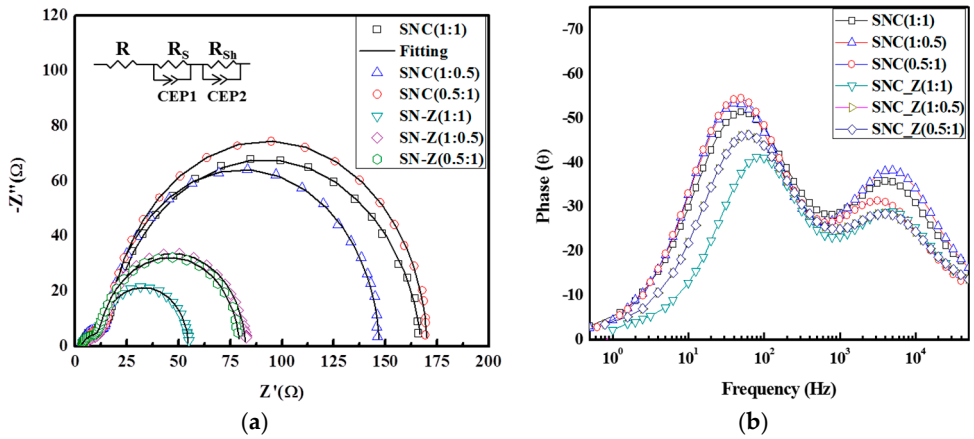

Figure 8. (**a**) Impedance spectra; and (**b**) bode phase plots of the DSSCs based on different photoanodes.

Table 2. Equivalent circuit parameters, electron lifetime (τ_e), effective diffusion coefficient (D_{eff}), and effective diffusion length (L_e) of the DSSCs based on different photoanodes.

Sample	R_s (Ω)	R_{sh} (Ω)	τ_e (ms)	D_{eff} ($cm^2 \cdot S^{-1}$)	L_e (cm)
SNC (1:1)	12.75	151.1	10.04	1.95×10^{-5}	0.447
SNC (1:0.5)	12.35	131.9	12.65	1.38×10^{-5}	0.422
SNC (0.5:1)	12.72	153.6	12.65	1.56×10^{-5}	0.499
SNC_Z (1:1)	9.02	69.33	3.99	4.90×10^{-5}	0.559
SNC_Z (1:0.5)	9.16	69.33	6.33	3.04×10^{-5}	0.555
SNC_Z (0.5:1)	9.16	67.38	7.97	2.35×10^{-5}	0.547

The charge transport resistances, R_{sh}, for SNC_Z (1:1) and SNC photoanodes were 69.33 Ω and 151.1 Ω, respectively, and the R_s of the SNC_Z (1:1) photoanode decreased from 12.75 Ω to 9.02 Ω as the LZO layer was coated on the top of the SNC photoanode. The EIS result demonstrated that the electron density increased in the conduction band of the SNC_Z photoanode and reduced the inter nanostructure resistance after introducing the LZO as the insulating layer. The electron lifetime (τ_e) in the photoanode is inversely proportional to the frequency of the maximum phase at the ω_2 component (ω_{max}), as shown in Equation (2) [38]:

$$\tau_e = 1/\omega_{max} = 1/K_{eff} \quad (2)$$

where K_{eff} is first-order reaction rate that constant for electrons being lost.

The energy conversion efficiency of the SNC_Z photoanode was higher than of the SNC photoanode because the electron lifetime of the SNC_Z was higher than that of the SNC photoanode with the LZO layer coated on the top of the SNC photoanodes, causing a low recombination reaction. However, the injected electron density of the SNC_Z photoanodes was higher than that of the SNC photoanode, and the LZO layer acted as an energy barriers, thus preventing prevent the electrons from returning from the surface of LZO and suppressing the recombination. The effective diffusion coefficient (D_{eff}) of an electron is another crucial factor that affects the efficiency of the DSSCs according to Equation (3) [39] (Table 2).

$$D_{eff} = \left(\frac{R_{sh}}{R_s}\right) \times L^2 \times K_{eff} \quad (3)$$

The SNC_Z photoanodes had a higher effective diffusion coefficient than the SNC photoanodes because the LZO layer affected the electron transport pathway. To explain the high current density in the SNC_Z photoanodes, the effective diffusion length (L_e) was calculated using Equation (4):

$$L_e = L_n \times L \quad (4)$$

where the value of the electron diffusion length (L_n) reflects the competition between charge collection and recombination.

$$L_n = \sqrt{D_{eff} \times \tau_e} \quad (5)$$

A long electron diffusion length confirms the quantitative collection of photo-generated charge carriers [40]. The SNC_Z (1:1) photoanode with a high L_e value of 0.559 exhibited the highest J_{sc} value of 4.73 mA/cm^2.

3. Materials and Methods

In this experiment, SNFs were prepared using a hydrothermal method. Details of the preparation of SNFs are provided elsewhere [41]. 0.188 M $Na_2SnO_3 \cdot 3H_2O$ (A18611, Alfa Aesar, Heysham, UK) and 0.35 M NaOH (A18395, Alfa Aesar) were mixed in a 40 mL aqueous solution at room temperature; 40 mL of absolute ethanol was then added drop-wise and the solution was stirred for 30 min. This solution was transferred to a stainless steel autoclave and then placed in a furnace at 200 °C for 48 h. It was then cooled down to room temperature. A precipitate was formed. The precipitate was centrifuged at 6000 rpm for 5 min, washed twice with deionized water and ethanol, and dried at 105 °C overnight.

LZO seed was prepared through a hydrolysis condensation reaction [42]. In brief, 0.01 M lithium acetate monohydrate ($LiAc \cdot 2H_2O$, 213195, Sigma-Aldrich, St. Louis, MO, USA) was used to dope 0.1 M zinc acetate dihydrate ($Zn(CH_3COO)_2 \cdot 2H_2O$ 4296, J.T.Baker, Phillipsburg, NJ, USA), which was then added to 250 mL of diethylene glycol. The solution was heated at 160 °C for 2 h and cooled to room temperature. A colloidal suspension was formed. The colloid was concentrated by a sequential treatment of centrifugation (6000 rpm for 5 min). The precipitate (ZnO aggregates) was finally dispersed in absolute ethanol and ultrasonicated for 20 min to obtain the final colloidal suspension solution.

SNC photoanodes were prepared by mixing SNF and commercially available SNPs (44606, Alfa Aesar) at various weight ratios of 1:1, 1:0.5 and 0.5:1 in absolute ethanol. In this study, SNC photoanodes with 1:1, 1:0.5 and 0.5:1 weight percentages of SNFs and SNPs were referred to as SNC (1:1), SNC (1:0.5), and SNC (0.5:1), respectively. SNC and LZO films were prepared by using a spin-coating technique, followed by annealing at high temperature. First, wet SNC films were coated on FTO and heated at 350 °C for 1 h. Then LZO insulating layer films were deposited on the top of the SNC films and annealed at 450 °C for 2 h. The SNC samples coated with the LZO insulating layer are referred to as SNC_Z (1:1), SNC_Z (1:0.5), and SNC_Z (0.5:1), respectively.

Next, 0.5 mM ethanolic solution of the ruthenium complex *cis*-bis(2,2-bipyridyl-4, 4-dicarboxylato)-ruthenium(II)-bis-tetrabutylammonium (commercially known as N719 dye($C_{58}H_{86}N_8O_8RuS_2$) (Esolar D719, Everlight, Taoyuan, Taiwan) was heated at 50 °C for 1 h in an ultrasonicator. Photoanode samples were heated at 100 °C for 1 h and then immersed in the N719 dye in the dark for 30 min. After 30-min dye adsorption, the sensitized films were rinsed with acetonitrile to remove excess dye from the surface, and the films were dried at 70 °C for 30 min. The sensitized photoanode was incorporated into a typical cell; a Pt counter-electrode was placed over the dye-sensitized photoanode, and the photoelectrochemical properties of the DSSC were measured. An Eversolar E5A electrolyte (Everlight) was injected into the space between the photoanode and counter-electrode.

The photocurrent-voltage characteristics were measured under one sunlight illumination irradiated by AM 1.5 G solar simulator (YSS-50A, Yamashita Denso, Tokyo, Japan). The active area of the resultant cell exposed to light was 0.25 cm^2. A photovoltaic analyzer (5500, Jiehan, Taichung, Taiwan) was used to control the output voltage of the DSSCs and record the current density. Maximum voltage obtained for a DSSC under one sun light illumination is the open circuit voltage, V_{oc}, and the short-circuit current, J_{sc}, is the current passing through the solar cell when the voltage across the solar cell is zero (i.e., when the solar cell is short circuited). A dual-channel optical meter (Model 96000, Newport, CA, USA) was used to measure the *IPCE*. Dark current measurements were performed by turning off the solar simulator light with a potential difference of 1.0 V. OCVD experiments were conducted by monitoring the subsequent decay of V_{oc} after stopping the illumination on DSSC under open circuit conditions.

The morphology was analyzed using a SEM (JSM-6701F, JEOL, Tokyo, Japan). A XRD (D-MAX, Rigaku, Tokyo, Japan) with Cu Kα radiation (λ = 0.15406 nm) at a low scan rate of 1° min^{-1} was used to analyze the structure of the samples. EIS measurements were performed using frequency response analyzer (1255B, Solartron, Leicester, UK) and potentiostat (1287A, Solartron) at a frequency ranging from 0.1 Hz to 100 KHz with an alternating current (AC) amplitude of 10 mV under one sun light illumination.

4. Conclusions

In summary, we successfully prepared a LZO insulating layer on the top of SNC photoanodes with different weight ratios of SNPs and SNFs. The conversion efficiency of DSSCs based on this novel photoanode microstructure was clearly increased. The SNPs increased the interconnection between SNFs and the FTO substrate. The DSSC based on the SNC_Z (1:1) photoanode exhibited a high efficiency (η) of 2.07%, which was considerably higher than that of the DSSCs based on the SNC (1:1) photoanode (0.7%). The performance of the DSSCs depended on the ratio of SNPs and SNFs and the LZO layer coating. The LZO layer coated on the top of the SNC photoanodes successfully suppressed the recombination in the photoanode and this was proven by the dark current, OCVD, and AC impedance measurements.

Acknowledgments: Financial support for this work was provided by the National Science Council of Taiwan under contract No. NSC 99-2221-E-155-028.

Author Contributions: Ripon Bhattacharjee carried out the experimental, analysis and wrote the manuscript under supervision of I-Ming Hung. All authors read and approved the final manuscript.

Conflicts of Interest: The authors declare no conflicts of interest.

References

1. Bella, F.; Galliano, S.; Gerbaldi, C.; Viscardi, G. Cobalt-based electrolyte for dye-sensitized solar cells: Recent advances towards stable devices. *Energies* **2016**, *9*, 384. [CrossRef]
2. Raj, A.C.; Prasanth, R. A critical review of recent developments in nanomaterials for photoelectrodes in dye sensitized solar cells. *J. Power Sources* **2016**, *317*, 120–132. [CrossRef]

3. Gerosa, M.; Sacco, A.; Scalia, A.; Bella, F.; Chiodoni, A.; Quaglio, M.; Tresso, E.; Bianco, S. Toward totally flexible dye-sensitized solar cells based on titanium grids and polymeric electrolyte. *IEEE J. Photovolt.* **2016**, *6*, 498–505. [CrossRef]
4. Bella, F.; Leftheriotis, G.; Griffini, G.; Syrrokostas, G.; Turri, S.; Gratzel, M.; Gerbaldi, C. A new design paradigm for smart windows: Photocurable polymer for quasi-solid photoelectrochromic devices with excellent long-term stability under real outdoor operating conditions. *Adv. Funct. Mater.* **2016**, *26*. [CrossRef]
5. Yella, A.; Lee, H.W.; Tsao, H.N.; Yi, C.; Chandiran, A.K.; Nazeeruddin, M.K.; Diau, E.W.G.; Yeh, C.Y.; Zakeeruddin, S.M.; Grätzel, M. Porphyrin-sensitized solar cells with cobalt (II/III)-based redox electrolyte 719 exceed 12 percent efficiency. *Science* **2011**, *334*, 629–634. [CrossRef] [PubMed]
6. Venditti, I.; Barbero, N.; Russo, M.V.; Di Carlo, A.; Decker, F.; Fratoddi, I.; Barolo, C.; Dini, D. Electrodeposited ZnO with squaraine sensitizers as photoactive anode of DSCs. *Mater. Res. Exp.* **2014**, *1*. [CrossRef]
7. Lee, J.H.; Park, N.G.; Shin, Y.J. Nano-grain SnO_2 electrodes for high conversion efficiency SnO_2-DSSC. *Sol. Energy Mater. Sol. Cells* **2011**, *95*, 179–183. [CrossRef]
8. Tan, B.; Toman, E.; Li, Y.; Wu, Y. Zinc stannate (Zn_2SnO_4) dye-sensitized solar cells. *J. Am. Chem. Soc.* **2007**, *129*, 4162–4163. [CrossRef] [PubMed]
9. Elumalai, N.K.; Jose, R.; Archana, P.S.; Chellappan, V.; Ramakrishna, S. Charge transport through electrospun SnO_2 nanoflowers and nanofibers: Role of surface trap density on electron transport dynamics. *J. Phys. Chem. C* **2012**, *116*, 22112–22120. [CrossRef]
10. Fonstad, C.G.; Rediker, R.H. Electrical properties of high quality stannic oxide crystals. *J. Appl. Phys.* **1971**, *42*, 2911–2918. [CrossRef]
11. Lupan, O.; Chowa, L.; Chaic, G.; Schultea, A.; Parka, S.; Heinrich, H. A rapid hydrothermal synthesis of rutile SnO_2 nanowires. *Mater. Sci. Eng. B* **2009**, *157*, 101–104. [CrossRef]
12. Bhande, S.S.; Taur, G.A.; Shaikh, A.V.; Joo, O.S.; Sung, M.M.; Mane, R.S.; Ghule, A.V.; Han, S.H. Structural analysis and dye-sensitized solar cell application of electrodeposited tin oxide nanoparticles. *Mater. Lett.* **2012**, *79*, 29–31. [CrossRef]
13. Liu, M.; Yang, J.; Feng, S.; Zhu, H.; Zhang, J.; Li, G.; Peng, J. Composite photoanodes of Zn_2SnO_4 nanoparticles modified SnO_2 hierarchical microspheres for dye-sensitized solar cells. *Mater. Lett.* **2012**, *76*, 215–218.
14. Milan, R.; Selopal, G.S.; Epifani, M.; Natile, M.M.; Sberveglieri, G.; Vomiero, A.; Concina, I. ZnO@SnO_2 engineered composite photoanodes for dye sensitized solar cells. *Sci. Rep.* **2015**, *5*, 14523. [CrossRef] [PubMed]
15. Tennakone, K.; Bandara, J.; Bandaranayake, P.K.M.; Kumara, G.R.A.; Konno, A. Enhanced efficiency of a dye-sensitized solar cell made from MgO-coated nanocrystalline SnO_2. *Jpn. J. Appl. Phys.* **2001**, *40*, L732–L734. [CrossRef]
16. Look, D.C.; Reynolds, D.C.; Sizelove, J.R.; Jones, R.L.; Litton, C.W.; Cantwell, G.; Harsch, W.C. Electrical properties of bulk ZnO. *Solid State Commun.* **1998**, *105*, 399–401. [CrossRef]
17. Wang, H.; Bhattacharjee, R.; Hung, I.M.; Li, L.; Zeng, R. Material characteristics and electrochemical performance of Sn-doped ZnO spherical-particle photoanode for dye-sensitized solar cells. *Electrochim. Acta* **2013**, *111*, 797–801. [CrossRef]
18. Polat, I.; Yılmaz, S.; Bacaksız, E.; Atasoy, Y.; Tomakin, M. Synthesis and fabrication of Mg-doped ZnO-based dye-synthesized solar cells. *J. Mater. Sci. Mater. Electron.* **2014**, *25*, 3173–3178. [CrossRef]
19. Bhattacharjee, R.; Hung, I.M. Effect of different concentration Li-doping on the morphology, defect and photovoltaic performance of Li-ZnO nanofibers in the dye-sensitized solar cells. *Mater. Chem. Phys.* **2014**, *143*, 693–701. [CrossRef]
20. Lai, F.I.; Yang, J.F.; Kuo, S.Y. Efficiency enhancement of dye-sensitized solar cells' performance with ZnO nanorods grown by low-temperature hydrothermal reaction. *Materials* **2015**, *8*, 8860–8867. [CrossRef]
21. EI-Morshedi, N.; Alzahrani, I.; Kizibash, N.A.; Al-Fayez, H.A.A. Toxic effect of zinc oxide nanoparticles on some organs in experimental male wistar rats. *Int. J. Adv. Res.* **2014**, *2*, 907–915.
22. Zhang, X.Q.; Yin, L.H.; Tang, M.; Pu, Y.P. ZnO, TiO_2, SiO_2, and Al_2O_3 nanoparticles induced toxic effects on human fetal lung fibroblasts. *Biomed. Environ. Sci.* **2011**, *24*, 661–669. [PubMed]
23. Cox, A.; Venkatachalam, P.; Sahi, S.; Sharma, N. Silver and titanium dioxide nanoparticle toxicity in plants: A review of current research. *Plant Physiol. Biochem.* **2016**, *107*, 147–163. [CrossRef] [PubMed]
24. Bhattacharjee, R.; Hung, I.M. A SnO_2 and ZnO nanocomposite photoanodes in dye-sensitized solar cells. *Electrochem Solid State Lett.* **2013**, *2*, Q101–Q104. [CrossRef]

25. Snaith, H.J.; Ducati, C. SnO_2-based dye-sensitized hybrid solar cells exhibiting near unity absorbed photon-to-electron conversion efficiency. *Nano Lett.* **2010**, *10*, 1259–1265. [CrossRef] [PubMed]
26. Frank, A.J.; Kopidakis, N.; Lagemaat, J.V.D. Electrons in nanostructured TiO_2 solar cells: Transport, recombination and photovoltaic properties. *Coord. Chem. Rev.* **2004**, *248*, 1165–1179. [CrossRef]
27. Tennakone, K.; Jayaweera, P.V.V.; Bandaranayake, P.K.M. Dye-sensitized photoelectrochemical and solid-state solar cells: Charge separation, transport and recombination mechanisms. *J. Photochem. Photobiol. A Chem.* **2003**, *158*, 125–130. [CrossRef]
28. Ito, S.; Liska, P.; Comte, P.; Charvet, R.; Pechy, P.; Bach, U.; Schmidt-Mende, L.; Zakeeruddin, S.M.; Kay, A.; Nazeeruddin, M.K.; et al. Control of dark current in photoelectrochemical (TiO_2/I^--I_3^-) and dye-sensitized solar cells. *Chem. Commun.* **2005**, *34*, 4351–4353. [CrossRef] [PubMed]
29. Hu, F.Y.; Xia, Y.J.; Guan, Z.S.; Yin, X.; He, T. Low temperature fabrication of ZnO compact layer for high performance plastic dye-sensitized ZnO solar cells. *Electrochim. Acta* **2012**, *69*, 97–101. [CrossRef]
30. Tan, B.; Wu, Y. Dye-sensitized solar cells based on anatase TiO_2 nanoparticle/nanowire composites. *J. Phys. Chem. B* **2006**, *110*, 15932–15938. [CrossRef] [PubMed]
31. Grätzel, M. Photoelectrochemical cells. *Nature* **2001**, *414*, 338–344. [CrossRef] [PubMed]
32. Bisquert, J.; Zaban, A.; Greenshtein, M.; Mora-Seró, I. Determination of rate constants for charge transfer and the distribution of semiconductor and electrolyte electronic energy levels in dye-sensitized solar cells by open circuit photovoltage decay method. *J. Am. Chem. Soc.* **2004**, *126*, 13550–13559. [CrossRef] [PubMed]
33. Chi, C.F.; Cho, H.W.; Teng, H.; Chuang, C.Y.; Chang, Y.M.; Hsu, Y.J.; Lee, Y.L. Energy level alignment, energy level alignment, electron injection, and charge recombination characteristics in CdS/CdSe cosensitized TiO_2 photoelectrode. *Appl. Phys. Lett.* **2011**, *98*. [CrossRef]
34. Santiago, F.F.; Canadas, J.G.; Palomares, E.; Clifford, J.N.; Haque, S.A.; Durrant, J.R.; Belmonte, G.G.; Bisquert, J. The origin of slow electron recombination processes in dye-sensitized solar cells with alumina barrier coatings. *J. Appl. Phys.* **2004**, *96*, 6903–6907. [CrossRef]
35. Saito, M.; Fujihara, S. Large photocurrent generation in dye-sensitized ZnO solar cells. *Energy Environ. Sci.* **2008**, *1*, 280–283. [CrossRef]
36. Dong, H.P.; Wang, L.D.; Gao, R.; Ma, B.B.; Qiu, Y. Constructing nanorod-nanoparticles hierarchical structure at low temperature as photoanodes for dye-sensitized solar cells: Combining relatively fast electron transport and high dye-loading together. *J. Mater. Chem.* **2011**, *21*, 19389–19394. [CrossRef]
37. Guerin, V.M.; Magne, C.; Pauporte, T.; Le Bahers, T.; Rathousky, J. Electrodeposited nanoporous versus nanoparticulate ZnO films of similar roughness for dye-sensitized solar cell applications. *ACS Appl. Mater. Interfaces* **2010**, *2*, 3677–3685. [CrossRef] [PubMed]
38. Liu, Y.; Sun, X.; Tai, Q.; Hu, H.; Chen, B.; Huang, N.; Sebo, B.; Zhao, X.Z. Efficiency enhancement in dye-sensitized solar cells by interfacial modification of conducting glass/mesoporous TiO_2 using a novel ZnO compact blocking film. *J. Power Sources* **2011**, *196*, 475–481. [CrossRef]
39. Adachi, M.; Sakamoto, M.; Jiu, J.; Ogata, Y.; Isoda, S. Determination of parameters of electron transport in dye-sensitized solar cells using electrochemical impedance spectroscopy. *J. Phys. Chem. B* **2006**, *110*, 13872–13880. [CrossRef] [PubMed]
40. Wang, M.; Chen, P.; Humphry-Baker, R.; Zakeeruddin, S.M.; Gratzel, M. The influence of charge transport and recombination on the performance of dye-sensitized solar cells. *Chemphyschem* **2009**, *10*, 290–299. [CrossRef] [PubMed]
41. Supothina, S.; Rattanakam, R.; Vichaphund, S.; Thavorniti, P. Effect of synthesis condition on morphology and yield of hydrothermally grown SnO_2 nanorod clusters. *J. Eur. Ceram. Soc.* **2011**, *31*, 2453–2458. [CrossRef]
42. Zhang, Q.; Dandeneau, C.S.; Candelaria, S.; Liu, D.; Garcia, B.B.; Zhou, X.; Jeong, Y.H.; Cao, G. Effects of lithium ions on dye-sensitized ZnO aggregate solar cells. *Chem. Mater.* **2010**, *22*, 2427–2433. [CrossRef]